Insights into Second-Sphere Effects on Redox Potentials, Spectroscopic Properties, and Superoxide Dismutase Activity of Manganese Complexes with Schiff-Base Ligands

Claudia Palopoli, Joaquín Ferreyra, Amandine Conte-Daban, Micaela Richezzi, Ana Foi, Fabio Doctorovich, Elodie Anxolabéhère-Mallart, Christelle Hureau, Sandra Signorella

ACS OMEGA

Article

Cite This: ACS Omega 2019, 4, 48−57

http://pubs.acs.org/journal/acsodf

Insights into Second-Sphere Effects on Redox Potentials, Spectroscopic Properties, and Superoxide Dismutase Activity of Manganese Complexes with Schiff-Base Ligands

Claudia Palopoli,[†] Joaquín Ferreyra,[†] Amandine Conte-Daban,[‡] Micaela Richezzi,[†] Ana Foi,[§] Fabio Doctorovich,[§] Elodie Anxolabéhère-Mallart,[∥] Christelle Hureau,[‡] and Sandra R. Signorella*[,†]

[†]IQUIR (Instituto de Química Rosario), Consejo Nacional de Investigaciones Científicas y Técnicas (CONICET), Facultad de Ciencias Bioquímicas y Farmacéuticas, Universidad Nacional de Rosario, Suipacha 531, S2002LRK Rosario, Argentina

[‡]LCC-CNRS, Université de Toulouse, 205 route de Narbonne, 31077 Toulouse, France

[§]Departamento de Química Inorgánica, Analítica y Química Física/INQUIMAE-CONICET, Facultad de Ciencias Exactas y Naturales, Universidad de Buenos Aires, Ciudad Universitaria, Pabellón 2, C1428EHA Buenos Aires, Argentina

[∥]Laboratoire d'Electrochimie Moléculaire UMR CNRS-P7 7591, Université Paris Diderot-Paris, 15 rue Jean-Antoine de Baïf, 75205 Paris Cedex 13, France

Supporting Information

ABSTRACT: Six Mn-Schiff base complexes, $[Mn(X\text{-salpn})]^{0/+}$ (salpn = 1,3-bis(sal-ic-ylidenamino)propane, X = H [**1**], 5-Cl [**2**], 2,5-F_2 [**3**], 3,5-Cl_2 [**4**], 5-NO_2 [**5**], 3,5-$(NO_2)_2$ [**6**]), were synthesized and characterized in solution, and second-sphere effects on their electrochemical and spectroscopic properties were analyzed. The six complexes catalyze the dismutation of superoxide with catalytic rate constants in the range 0.65 to 1.54×10^6 M^{-1} s^{-1} obtained through the nitro blue tetrazolium photoreduction inhibition superoxide dismutases assay, in aqueous medium of pH 7.8. In solution, these compounds possess two labile solvent molecules in the axial positions favoring coordination of the highly nucleophilic $O_2^{\bullet-}$ to the metal center. Even complex **5**, [Mn(5-(NO_2)salpn) (OAc) (H_2O)], with an axial acetate in the solid state, behaves as a 1:1 electrolyte in methanolic solution. Electron paramagnetic resonance and UV−vis monitoring of the reaction of $[Mn(X\text{-salpn})]^{0/+}$ with KO_2 demonstrates that in diluted solutions these complexes behave as catalysts supporting several additions of excess $O_2^{\bullet-}$, but at high complex concentrations (≥0.75 mM) catalyst self-inhibition occurs by the formation of a catalytically inactive dimer. The correlation of spectroscopic, electrochemical, and kinetics data suggest that second-sphere effects control the oxidation states of Mn involved in the $O_2^{\bullet-}$ dismutation cycle catalyzed by complexes **1**−**6** and modulate the strength of the Mn-substrate adduct for electron-transfer through an inner-sphere mechanism.

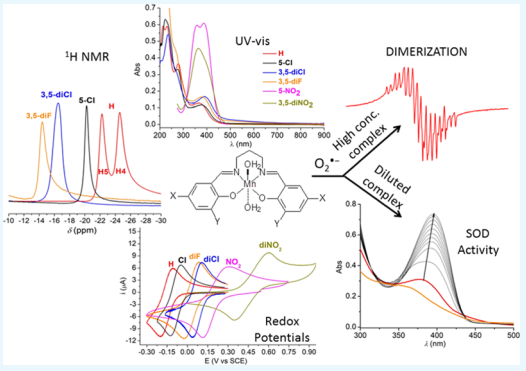

INTRODUCTION

The superoxide radical anion ($O_2^{\bullet-}$) is generated by the one-electron reduction of O_2 during normal cellular metabolism and constitutes the primary source of the deleterious hydroxyl radical ($HO^{\bullet}$) and hydrogen peroxide (H_2O_2). Manganese superoxide dismutases (SODs) catalyze the conversion of intracellular $O_2^{\bullet-}$ into O_2 and H_2O_2 and constitute one of the major antioxidant defense systems against this toxic metabolite.[1] The active site of these enzymes contains one Mn ion bound to three histidine ligands, one aspartate and water or hydroxide as the fifth ligand in a trigonal bipyramidal geometry, and carries out $O_2^{\bullet-}$ disproportionation through a redox process involving one-electron oxidation and reduction of the metal ion between Mn(II)/Mn(III) levels.[2] In a number of neurodegenerative and cardiovascular diseases, the production of reactive oxygen species (ROS) exceeds the antioxidant defenses and results in tissue injuries.[3,4] In this context, efforts have been directed toward the search of low-molecular-weight SODs mimics as catalytic agents for the prevention of oxidative stress disturbances.[5−8] Several Mn-based complexes have shown protective efficacy for ROS-associated pathologies[9,10] and better bioavailability than exogenous SOD enzymes.[11] Among them, Mn complexes of the salen (1,2-bis(salicylidenamino)ethane) family have been tested in several animal models.[12−14] The SOD activity of mononuclear Mn-Schiff-base complexes has been extensively studied.[15] However, the mechanism of the catalyzed $O_2^{\bullet-}$ dismutation by these compounds, the influence of second-sphere effects—

Received: October 30, 2018
Accepted: December 20, 2018
Published: January 2, 2019

DOI: 10.1021/acsomega.8b03018
ACS Omega 2019, 4, 48−57

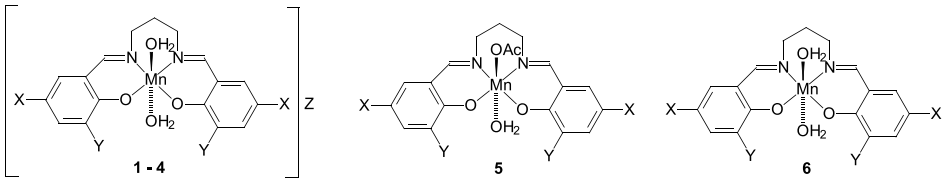

Figure 1. Complexes studied in this work. **1**: X = Y = H, Z = ClO_4; **2** : X = Cl, Y = H, Z = ClO_4; **3** X = Y = F, Z = BPh_4; **4**: X = Y = Cl, Z = ClO_4; **5**: X = NO_2, Y = H; **6**: X = Y = NO_2.

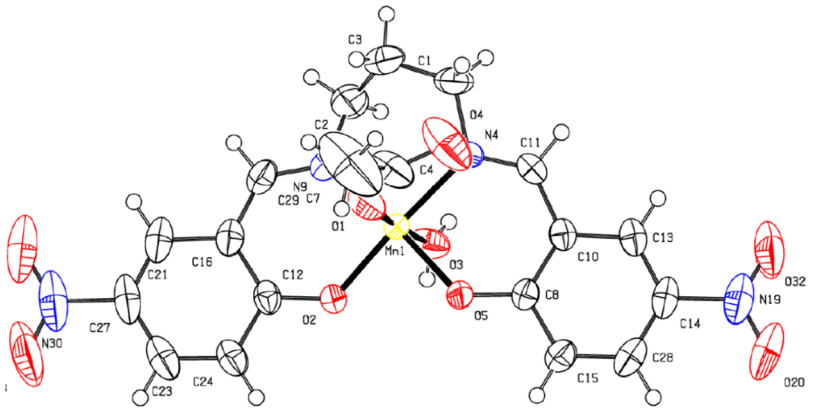

Figure 2. Plot of the asymmetric unit of **5** at the 50% probability level. Selected bond lengths (Å) and angles (°): Mn(1)−O(1) 2.126(2), Mn(1)−O(2) 1.901(1), Mn(1)−O(3) 2.306(2), Mn(1)−O(5) 1.898(1), Mn(1)−N(4) 2.024(2), Mn(1)−N(9) 2.010(2), O(2)−Mn(1)−N(4) 175.38(7), O(5)−Mn(1)−N(9) 169.67(8), O(1)−Mn(1)−O(3) 175.70(7).

which can be crucial for determining the reactivity of biomimetic metal complexes,[16,17] and even the oxidation states involved in the catalytic cycle remain exiguously understood. Although a Mn(II)/Mn(III) cycle during catalysis has been invoked,[18] the key features for their activity (intermediates or active species formed upon reaction with $O_2^{\bullet-}$) are still elusive. In this work, we try to answer two questions that remain open: do the Mn-Schiff base complexes react with $O_2^{\bullet-}$ through an outer or inner sphere mechanism? Are the redox potential of these complexes key for their reactivity? For this, we correlate the redox and spectroscopic properties of a series of Mn-X-salpn complexes (Figure 1) with their SOD activity, aimed at unraveling some clues for their mode of action to face $O_2^{\bullet-}$.

RESULTS AND DISCUSSION

Characterization of the Complexes. X-ray structures of complexes **1**−**4** have been reported previously. In these compounds, the metal ion is in the Mn(III) oxidation state with the ligand disposed in the equatorial plane and two capping water molecules occupying the trans-diapical positions.[19−23] The IR spectra of these complexes show the fingerprint typical of the ligands with the C═N bond stretching shifted to frequencies lower than in the ligand denoting coordination to the metal ion and intense bands corresponding to the counter anions (Figure S1). In aqueous or methanolic solution, these complexes behave as 1:1 electrolytes and can be formulated as $[Mn(X\text{-salpn})(solv)_2]^+$. Electrospray ionization (ESI)-mass spectra of the complexes in methanol show one main peak (positive mode, Figure S2) belonging to $[Mn(X\text{-salpn})]^+$, and the paramagnetic ^1H NMR spectra of the four compounds in D_4-methanol exhibit a common pattern outside the diamagnetic region (Figure S3). One broad signal at 19 ppm attributed to the central methylene of the $-(CH_2)_3-$ aliphatic chain, and one (H4/H4′ in **2**, **3**, **4**) or two (H4/H4′ and H5/H5′ in **1**) upfield resonances belonging to the aromatic ring protons, a probe for the symmetrically arranged tetradentate Schiff-base ligand in the equatorial plane.[24,25] The −N═CH− imino H appears at −95 ppm for complex **1** and −106 ppm for **4** (shown in the inset of Figure S3). Other protons adjacent to the donor groups of the Schiff base ligand (aromatic H3/H3′ and H6/H6′ and $-CH_2-N=C$) are not observed in the ^1H NMR spectra (rapid relaxation or very large chemical shift).[19,24,26]

Complex **5** was synthesized by adding $Mn(OAc)_2{\cdot}4H_2O$ to the fully deprotonated ligand. Under these conditions, acetate binds to the Mn ion affording the neutral $[Mn(5\text{-}(NO_2)\text{-salpn})(OAc)(H_2O)]$ (**5**). The X-ray diffraction structure of **5** (not reported previously) shows the hexacoordinated Mn(III) center adopting a pseudotetragonal geometry, with the N_2O_2-donor atoms from the tetradentate 5-(NO_2)salpn ligand in the equatorial plane, and the apical positions occupied by one O atom from a monodentate acetate ion and one capping water molecule (Figure 2). The coordination sphere of Mn exhibits an elongated octahedral geometry, with the equatorial Mn−N/O bond distances ($Mn-O/N_{(av)}$ 1.958 Å) shorter than the apical Mn−O ones ($Mn-O_{(av)}$ 2.216 Å), typical of the Jahn−Teller distorted d^4 Mn(III) ion. The complex behaves as a 1:1 electrolyte in methanol, indicating that acetate dissociates in the protic solvent.

Complex **6** is a Mn(II) complex formulated as $[Mn(II)(3,5\text{-}(NO_2)_2\text{-salpn})(H_2O)_2]$, which in methanol behaves as a non-electrolyte (same conductivity as for the neat solvent), indicating that the compound remains neutral in solution. The ESI-mass spectrum of a solution of **6** in DMSO shows one main peak (positive mode, Figure S2) that can be assigned to the in situ oxidized $[Mn(3,5\text{-}(NO_2)_2\text{-salpn})(DMSO)(H_2O)]^+$ counterpart.

The oxidation state of Mn in the six compounds was confirmed by perpendicular-mode electron paramagnetic

DOI: 10.1021/acsomega.8b03018
ACS Omega 2019, 4, 48−57

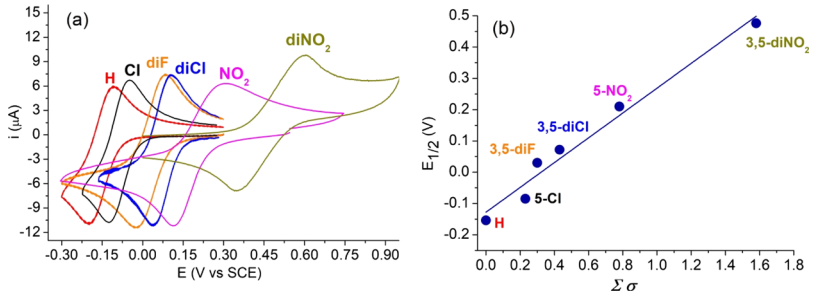

Figure 3. (a) Cyclic voltammogram of complexes **1**−**6** in DMF. Conditions: C/Pt/SCE; conc. = 1 mM; supporting electrolyte = Bu_4NPF_6, scan rate = 100 mV/s. (b) Plot of redox potentials of complexes in DMF against $\Sigma\sigma$.

Table 1. SOD Activity of 1−6 and Other Mn-Schiff Base Complexes, at pH 7.8[a]

complex[a]	IC_{50} (μM)	$10^6 \times k_{McF}$ M^{-1} s^{-1}	$E_{1/2}$ (Mn(III)/Mn(II)) V vs SCE	refs
1 (H)	1.48	1.53[b]	−0.153	this work
2 (5-Cl)	1.49	1.52[b]	−0.085	this work
3 (3,5-diF)	2.44	0.93[b]	0.030	this work
4 (3,5-diCl)	2.29	0.99[b]	0.071	this work
5 (5-NO_2)	3.51	0.65[b]	0.210	this work
6 (3,5-diNO_2)	1.96	1.16[b]	0.476	this work
[Mn(X-salen)]$^+$		0.6[c]	−0.237 to 0.031 (DMF)	39,41
[Mn(3-OMe-salenR)]$^+$		0.4−1.4[d]	−0.644 to 0.206 (DMSO)	42
[Mn(5-SO_3-salen)]$^-$		1.2[b]	0.199 (H_2O)	43
[Mn(5-SO_3-salpn)]$^-$		3.6[b]	−0.048 (MeOH)	43
[Mn(CysalenSO$_3$)]$^{2-}$		5.49[c]		44
[Mn(naphtophenSO$_3$)]		3.11[c]		45
[Mn(salbutO)]		1.91[b]	0.356 (DMF, Mn(III)/Mn(IV))	46
[Mn(pyr$_2$pn)]$^+$		1.84[b]		47
[Mn(pyr$_2$en)]$^+$		1.05[b]		47

[a]X = H, Cl, OMe. R = cyclopentane-fused with ureido or acid−base catalyst auxiliary. SO_3-CySalen = *N*,*N*′-bis(5-sulfonatosalicylidene)-(*R*,*R*)-1,2-diaminocyclohexane. Naphtophen = 1,2-bis((2-hydroxynaphthalen-1-yl)methyleneamino)benzene. SalbutOH = 1,4-bis(salicylidenamino)butan-2-ol. H_2Pyr_2pn = 1,2-bis(pyridoxylidenamino)propane. H_2Pyr_2en = 1,2-bis(pyridoxylidenamino)ethane. [b]Riboflavin−methionine−NBT assay. [c]Xanthine−xanthine oxidase−NBT assay. [d]Xanthine−xanthine oxidase−cytochrome c assay.

resonance (EPR) spectroscopy. Complexes **1**−**5** are EPR-silent in frozen DMSO solutions, a fact consistent with the presence of d^4 Mn(III) ions with high zero-field splitting values.[27,28] In contrast, complex **6** exhibits a six-line EPR signal (hyperfine splitting of ∼90 G) at g = 2 and two weak resonances on the low-field side at $g \approx 3$ and 5, characteristic of Mn(II) (shown below in Figure 8a) with zero-field splitting slightly weaker than the X-band microwave frequency.[29−32]

Effect of the Substituents on the Reduction Potentials of Complexes 1−6. Cyclic voltammetry was used to investigate the electrochemical properties of complexes **1**−**6** in dimethylformamide (DMF) (Figure 3). The six complexes exhibit a quasi-reversible wave corresponding to the Mn(III)/Mn(II) redox couple, with ΔE_p in the range 69−108 mV for complexes with unsubstituted and halogen-substituted ligands, and larger ΔE_p values for the nitro-derivatives (Table S1). For all the six complexes, the I_{pa}/I_{pc} ratio is within the range 0.89−1.00. These data indicate quasi-reversible electrochemical processes. The phenol ring substituents span the redox potentials ($E_{1/2}$, Table 1) of the Mn(III)/Mn(II) couple from −0.153 to 0.476 V versus saturated calomel electrode (SCE) as the electron-withdrawing ability of the substituent increases. The plot of $E_{1/2}$ versus the combined Hammett parameters of the substituents ortho and para to the phenolate ($\Sigma\sigma$)[33] yields an excellent linear correlation (Figure 3). This means that both substituents modulate the oxidation state of the Mn ion. This is especially evident for complex **6**, where the introduction of the second NO_2 group increases the potential enough to stabilize the Mn(II) oxidation state. Besides, for complex **5** it should be expected that the axial acetate has an effect on the Mn(III)/Mn(II) redox couple. However, the redox potential of **5** does not move away from the linear trend, suggesting that even in DMF the acetate dissociates.

Effect of the Substituents on the Charge Transfer Band in the Electronic Spectra. UV−vis spectroscopy shows that the substituent on the phenolato influences the energy of the charge transfer (CT) transitions of Mn-X-salpn complexes and provides a clear correlation between the ligand donor ability and the electron density of the metal center in these complexes. Electronic spectra of complexes **1**−**6** were registered in the aqueous phosphate buffer employed for the SOD tests (Figure 4a). Spectra taken immediately and 30 min (the illumination time used in the SOD tests) after preparation of solutions of **1**−**4** were virtually identical, meaning the complexes are stable in the buffer during the reaction time. Absorptions between 350 and 450 nm correspond to ligand to metal CT (LMCT) transitions from a pπ orbital of the phenolato oxygen to the partially filled dπ orbitals of the Mn ion.[34,35] For complexes **5** and **6**, the intense absorption bands of the nitro groups overlap the CT transitions and preclude their observation. The LMCT energy values across compounds **1**−**4** of this series decrease as the electron-withdrawing character of the substituents increases: 27 173 cm^{-1} (ε =

DOI: 10.1021/acsomega.8b03018
ACS Omega 2019, 4, 48−57

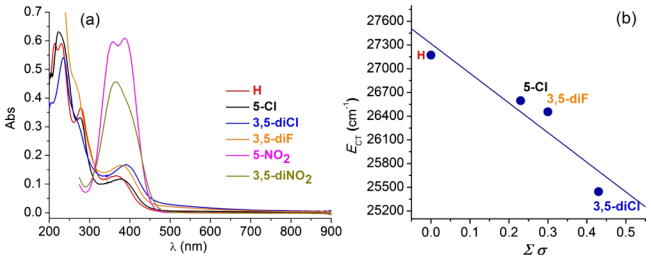

Figure 4. (a) Electronic spectra of complexes **1**–**6** in phosphate buffer of pH 7.8. [Complex] = 0.02 mM. (b) Plot of the energy of the LMCT bands of **1**–**4** against Σσ.

6450, **1** (H)) > 26 595 cm^{-1} (ε = 5900, **2** (5-Cl)) > 26455 cm^{-1} (ε = 8300, **3** (3,5-diF)) > 25 445 cm^{-1} (ε = 8350, **4** (3,5-diCl)). The plot of the LMCT energy values against the combined Hammett parameter of the substituents gives a good linear correlation (Figure 4b), highlighting these ligands are predominantly π-donor: the stronger the electron-withdrawal from the $O_{phenolato}$, the weaker π-donor ability of the ligand (partially filled dπ* orbitals lying at lower energy).

Effect of the Substituents on the Chemical Shift of the Aromatic H4/H4′ Protons in ^{1}H NMR Spectra of Complexes 1–4. The isotropically shifted NMR resonances of aromatic H4/H4′ protons of **1**–**4** in D_4-methanol are compared in Figure 5. Given the low solubility of complexes **5**

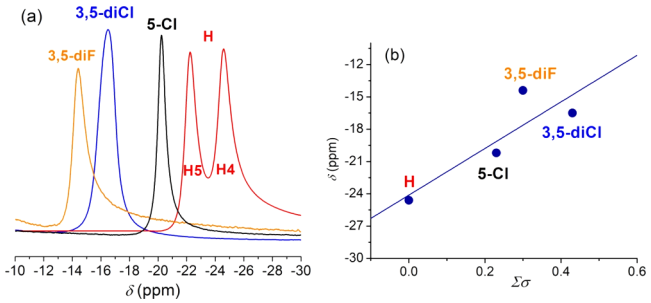

Figure 5. (a) Aromatic protons resonances in the ^{1}H NMR spectra of **1**–**4** in D_4-methanol. [complex] = 20 mM. (b) Plot of H4 chemical shift of **1**–**4** against Σσ.

and **6** in methanol, these compounds were not analyzed by this technique. As stated above, the ^{1}H NMR spectral pattern of **1**–**4** indicates that in solution these complexes retain the trans-diaxial geometry with the tetradentate Schiff-base ligand symmetrically arranged in the equatorial plane.[24,25,36,37] In these complexes, the phenolato protons are expected to be predominantly influenced by two contact shift pathways involving spin-delocalization onto the phenyl ring through the imino N-donor and phenolato O-donor atoms that generate upfield-shifted aromatic proton signals with large relaxation values.[24,38] The chemical shift of H4 correlates with the combined Hammett parameter of the substituents, moving downfield with the increased electron-withdrawal effect of the substituents. The H4 resonance can be used as a signature of the effect of substituent for this kind of compounds; therefore, more positive (or less negative) chemical shifts are expected for the NO_2-derivatives.

Effect of the Substituents on SOD Activity of 1–6. The redox potential of the six complexes fall in between the potentials for the $O_2^{\bullet-}$ one electron reduction and oxidation: $E(O_2^{\bullet-}/H_2O_2)$ = 0.642 V (vs SCE at pH 7) and $E(O_2/O_2^{\bullet-})$ = −0.404 V (vs SCE at pH 7), respectively, so they are expected to be active for $O_2^{\bullet-}$ dismutation. The SOD activity of complexes **1**–**6** was evaluated in phosphate buffer of pH 7.8 using an indirect assay, which involves inhibition of the reduction of nitro blue tetrazolium (NBT) by $O_2^{\bullet-}$. In this assay, reaction of photoreduced riboflavin with O_2 generates $O_2^{\bullet-}$ that converts the colorless NBT into purple formazan, measured at 560 nm. The SOD activity of the mimics is inversely related to the amount of formazan and the six complexes showed increasing inhibition of the reduction of NBT as their concentration raised (Figure 6a).

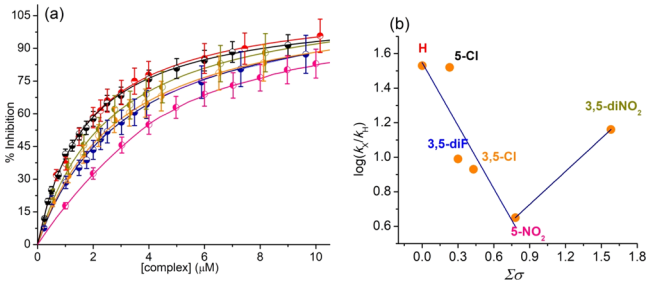

Figure 6. (a) SOD activity of complexes **1** (red), **2** (black), **3** (blue), **4** (orange), **5** (pink), and **6** (dark yellow) in the riboflavin–methionine–NBT assay. (b) Influence of the substituent in complexes **1**–**6** on k_{McF}.

The IC_{50} values (the concentration of the SOD mimic that diminishes by 50% the speed of reduction of NBT) were evaluated graphically and used to calculate the McCord–Fridovich second-order rate constants, $k_{McF} = k_{NBT}$ [NBT]/IC_{50} (Table 1). These k_{McF} values are independent of the detector concentration and suitable to compare with literature values.[39−47] Complexes **1**–**6** react faster than the Mn-X-salen analogues, for which only one k_{McF} value has been reported for the full series in spite of the variation in their redox potentials,[39−41] but react slower than water soluble Mn(III) complexes of sulfonato-derived Schiff base ligands even when the last are negatively charged.[43−45] In any case, Mn-Schiff base complexes with $-(CH_2)_3-$ spacer in the diimino fragment show higher SOD activity than analogues with the shorter $-(CH_2)_2-$ alkyl chain ([Mn(salpn)]$^+$ vs [Mn(salen)]$^+$; [Mn(5-SO_3-salpn)]$^-$ vs [Mn(5-SO_3-salen)]$^-$; Mn(pyr$_2$pn)]$^+$ vs [Mn(pyr$_2$en)]$^+$), probably because the bending of salpn ligands leads to a weakly coordinate exchangeable axial solvent molecule which favors substrate binding. Besides, the SOD activities of these Mn-Schiff base complexes are in the same range as for Mn-amine/pyridine complexes.[15,48]

The plot of $\log(k_X/k_H)$ against the combined Hammett parameters of substituents (Figure 6b), where k_X/k_H is the ratio between k_{McF} of X-substituted and the unsubstituted Mn complex, shows that the rate of the reaction of the Mn(III) complexes with $O_2^{\bullet-}$ decreases as the electron-withdrawal effect of the substituents increases. Because the complexes with the more electron-withdrawing substituents are more difficult to oxidize, the observed trend suggests that oxidation of the catalyst with simultaneous $O_2^{\bullet-}$ reduction should be the rate-limiting step in the reaction.[49,50] It must be noted that the diNO_2 complex (**6**) reacts faster than expected probably because this complex catalyzes $O_2^{\bullet-}$ dismutation through a different redox cycle (see below). On the other hand, the trans-effect of bound acetate in complex **5** is expected to increase the $O_2^{\bullet-}$ reaction rate.[51] However, it follows the trend and reacts

DOI: 10.1021/acsomega.8b03018
ACS Omega 2019, 4, 48−57

slower than complexes **1**−**4**. Dissociation of the apical acetate ligand in the aqueous buffer medium explains this, in line with its electrolytic behavior in methanol.

EPR and UV−Vis Monitoring of the Reaction of Mn-X-Salpn Complexes with KO_2. KO_2 is rather stable toward self-dismutation in DMSO, so this solvent was chosen to follow the reaction of Mn-X-salpn complexes with superoxide. We selected complexes **1** and **5** (with the highest and lowest k_{McF} values in this series) and **6** (in a different starting oxidation state) for the EPR monitoring of their reaction with KO_2. As stated before, **1** is EPR-silent in perpendicular mode, whereby this technique is particularly useful to detect species in different oxidation states generated during the redox reaction. [**1**]/[KO_2] 1:1 ratio was used in the EPR measurements. The 9 GHz band EPR spectra registered during and at the end of the reaction are shown in Figure 7. Thirty seconds

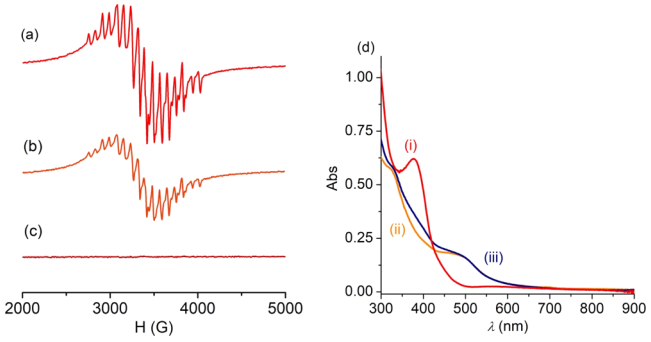

Figure 7. X-band EPR spectra of **1** + KO_2 in DMSO, (a) t = 27 s, (b) t = 1.5 min, and (c) at the end of the reaction. T = 115 K. (d) UV−vis spectra of (i) **1** in DMSO; (ii) mixture of **1** and KO_2 in DMSO, t = 40 min; (iii) [Mn(IV)(O)(salpn)]$_2$.

after addition of $O_2^{\bullet-}$ to 1.25 mM **1**, the EPR spectrum exhibits a 16-line signal centered at g = 2 typical of a di-μ-oxo-bridged Mn(IV)Mn(III) species.[31,52−55] The signal is still present at 1.5 min (Figure 7b) but its intensity decreases with time and finally disappears (Figure 7c). This final product could be a Mn(III), Mn(III)$_2$, or Mn(IV)$_2$ complex, inactive in EPR. To gain insight into the nature of the final product, the reaction of 1.25 mM **1** + 1.3 mM KO_2 was also monitored by UV−vis spectroscopy. The spectral pattern of the starting complex was immediately lost and new bands grew up (Figure 7d), with an intense absorption band around 500 nm characteristic of the formation of a bisoxo-bridged diMn(IV) dimer.[23,56] The spectral features of the spectrum of the reaction product are very close to those of an authentic sample of [Mn(O)(salpn)]$_2$ (Figure 7b(iii)) independently prepared and measured at the same final concentration as the diluted reaction mixture. The spectrum remained unchanged after 24 h, suggesting that this is the thermodynamic product of the reaction. Therefore, under these conditions (high concentration of complex), the monomer converts into the dimer quantitatively—as quantified spectrophotometrically against authentic [Mn(O)(salpn)]$_2$. The formation of [Mn(O)(salpn)]$_2$ was confirmed by ESI-MS (Figure S4). Under the same conditions, EPR monitoring of the reaction of **5** (0.75 mM) and KO_2 (1.1 mM) showed the growth up of the Mn(III)(μ-O)$_2$Mn(IV) 16-lines signal (Figure 8e) after a few minutes and its disappearance at longer times.

The reaction of **6** (1.6 mM) and KO_2 in DMSO was also monitored by EPR spectroscopy. The six-line signal of the

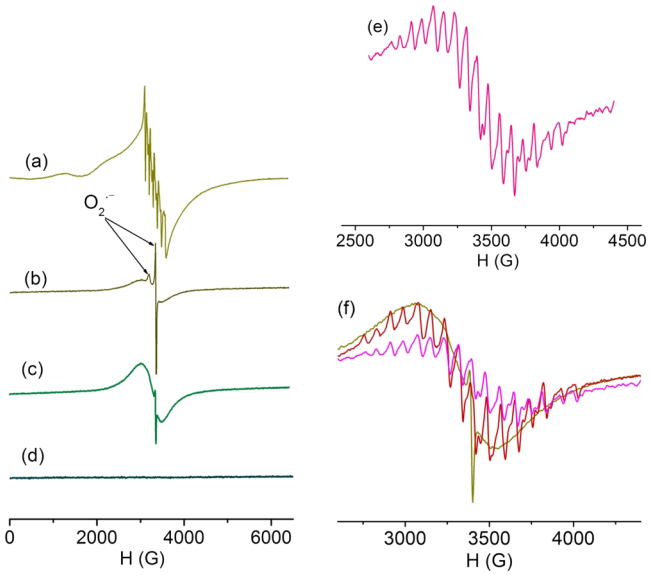

Figure 8. (a) X-band EPR spectra of **6** in DMSO; **6** + KO_2 in DMSO, (b) t = 20 s and (c) t = 2 min, and (d) after 1 day; (e) **5** + KO_2 in DMSO, t = 2 min 30 s; (f) comparison of EPR signals observed during the reaction of **1** (red), **5** (pink), and **6** (dark yellow) with KO_2 in DMSO. T = 115 K.

starting Mn(II) complex (Figure 8a) disappeared immediately after mixing and converted into a broad signal (width = 1260 G) centered at g = 2 (Figure 8b,c) that remained several minutes and then cleared up. In this case, solid KO_2 was added to the solution of complex in DMSO, so the signal of unreacted KO_2 ($g_{\parallel}$ = 2.1021, $g_{\perp}$ = 2.003)[57] is observed in the spectra. The $O_2^{\bullet-}$ signal is still present when the broad signal disappears and holds during several hours. The broad unresolved signal observed in the **6** + KO_2 reaction (the signals of intermediates formed by reaction of **1**, **5**, and **6** with KO_2 are compared in Figure 8f) suggests that the dimerization process does not occur through a Mn(III)Mn(IV) intermediate, as in the case of **1** and **5**.

To check if the formation of the dimer was related to the initial concentration of the starting complex, a more diluted sample of **1** was treated with KO_2 in DMSO and the reaction was followed spectrophotometrically. After addition of 1.5 mM KO_2 to 0.04 mM **1** in DMSO, the CT band of the starting complex (red line in Figure 9a) shifted 17 nm toward longer wave lengths (black lines in Figure 9a) and its intensity

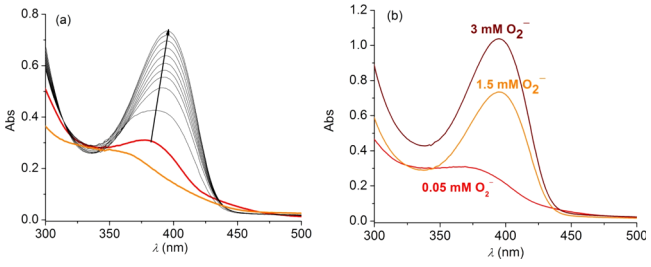

Figure 9. (a) Sequential electronic spectra during the reaction of **1** and KO_2 in DMSO. [**1**] = 0.04 mM; [KO_2] = 1.5 mM. Black lines: spectra taken during 40 min; red line: starting complex; orange line: spectrum registered after 24 h. (b) Compared UV−vis spectra for the reaction of 0.044 mM **1** and different concentrations of KO_2, registered 16 min after the reaction starts.

DOI: 10.1021/acsomega.8b03018
ACS Omega 2019, 4, 48−57

increased. The intensity of the band at 395 nm depends on $[O_2^{\bullet-}]$, growing with higher $[O_2^{\bullet-}]$ (Figure 9b). At longer times, this band vanishes and gives rise to a band shifted toward shorter wavelengths (orange line in Figure 9a) which remains unchanged with time. This final species, which could correspond to a Mn(III) dimer,[24] is still active, as second and third additions of excess KO_2 cause the growth of the band at 395 nm and consumption of KO_2.

Two important observations can be pointed out from these results: first, in the less concentrated solutions of **1**, the Mn(IV) dimer does not form (no band at 500 nm characteristic of a dimer is observed) and, second, the complex acts as a catalyst, because it reacts with excess $O_2^{\bullet-}$. Therefore, catalyst self-inhibition occurs at high complex concentrations by the formation of the catalytically inactive dimer, while in diluted solutions the complex behaves as a catalyst supporting several additions of excess $O_2^{\bullet-}$, which validates concentrations employed in the SOD assays.

Proposed Mechanism for the Reaction of Mn-X-Salpn Complexes with KO_2. A complex with the metal-centered redox couple closest to the midpoint between the oxidation and reduction of $O_2^{\bullet-}$ (0.12 V vs SCE) is expected to be a more potent SOD mimic than a complex with a farther redox potential.[15] This is essential when the reaction of $O_2^{\bullet-}$ with the complexes follows an outer sphere electron-transfer process. However, it seems not to be the case for Mn-X-salpn complexes because those complexes with redox potentials closed to 0.12 V react slower than **1** and **6**. The nucleophilicity of $O_2^{\bullet-}$ and the presence of labile solvent molecules in the axial positions of complexes **1**−**6** favor coordination of $O_2^{\bullet-}$ followed by an inner-sphere electron-transfer mechanism, such as observed for other Mn complexes with the ligand (either cyclic or acyclic) disposed in the equatorial plane.[58−60] In such a mechanism, the variation of the electronic properties of the substituents can control the dismutation rate by modulating the strength of the Mn−O bond in the $Mn-O_2^+$ adduct. Therefore, electron-withdrawing substituents attenuate the activity of the complex, giving rise to a weaker $Mn-O_2^+$ bond that leads to slower electron-transfer rate. It is expected that Mn-X-salpn complexes with electron-donor substituents lead to a stronger $Mn-O_2^+$ with higher activity. At present, we are performing density functional calculations on X-salpn-Mn^+ and X-salpn-Mn-O_2^+ to confirm this hypothesis. On the basis of spectroscopic and kinetic results, the mechanism of Scheme 1

Scheme 1. Proposed Mechanism for the Reaction of 1−5 with KO_2

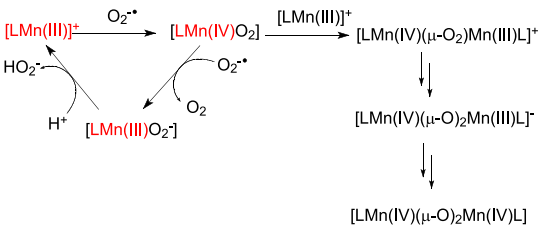

is proposed. At low complex concentrations, where the complexes catalyze $O_2^{\bullet-}$ dismutation, the starting complexes **1**−**5** may react with $O_2^{\bullet-}$ to form the Mn(IV)-peroxo adduct[61] which upon reaction with a second $O_2^{\bullet-}$ affords Mn(III)-peroxo and O_2. Proton-assisted release of HO_2^- can then take place to restore Mn(III).[62] This last step is fast in the aqueous medium of the SOD assay but much slower in DMSO, where the source of H^+ is the molecules of water originally present in the starting complexes. In DMSO, when the concentration of complex is ≥0.75 mM, the Mn(IV)-peroxo adduct formed in the first step can react with the Mn(III) complex to generate the Mn(III)Mn(IV) mixed valence complex (16-lines EPR spectra in Figures 7a and 8) by nucleophilic attack of the peroxo ligand on the Mn(III) center, which then evolves to the final Mn(IV) dimer (UV−vis spectrum in Figure 7d(ii)).

For **6**, a lower redox cycle is proposed (Scheme 2) based on the oxidation state of Mn in the starting complex and the high

Scheme 2. Proposed Mechanism for the Reaction of 6 with KO_2

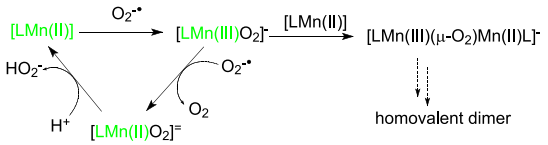

redox potential expected for the Mn(III)/Mn(IV) couple. In the first step, reaction of **6** with $O_2^{\bullet-}$ should lead to formation of a Mn(III)-peroxo adduct, which reacts with a second $O_2^{\bullet-}$ radical to generate O_2 and Mn(II)-peroxo, followed by protonation to restore Mn(II) and release of HO_2^-. At higher complex concentration, the formation of a Mn(III)Mn(II) mixed valence complex is also possible through the nucleophilic attack of the Mn(III)-peroxo to the Mn(II) center of **6**.[48,63] The disappearance of the broad signal in the EPR spectra taken at long times suggests that the mixed valence dimer finally yields a homovalent one, probably a Mn(III) dimer.

In conclusion, second-sphere effects of the substituents in Mn(III)-X-salpn complexes modulate the redox potentials of the metal center and the metal−ligand bond strength and guide their reactivity with $O_2^{\bullet-}$. Given the correlation between rates and redox potentials and the spectroscopic evidence for the formation of higher valence Mn complexes upon reaction with $O_2^{\bullet-}$, the dismutation of $O_2^{\bullet-}$ catalyzed by **1**−**5** is proposed to involve Mn(III)/Mn(IV) oxidation states through an inner-sphere mechanism, where coordination of superoxide is critical. In complex **6**, the two nitro groups shift the redox potential to positive values enough to catalyze $O_2^{\bullet-}$ dismutation through the Mn(II)/Mn(III) redox couple. Therefore, not only the redox potentials but also the coordination of superoxide are key for the SOD activity of these complexes.

METHODS

Synthesis of Complexes. Complexes, **1**·H_2O, **2**·H_2O, **3**·$3H_2O$, and **4**·$2H_2O$, were synthesized following procedures previously reported in refs 22, 23, and 64. Synthetic details for the obtention of the four compounds are described in the Supporting Information.

*Synthesis of [Mn(5-(NO_2)-salpn)(OAc)(H_2O)] (**5**).* A mixture of 5-(NO_2)salpnH_2 (310 mg, 0.83 mmol), $Mn(OAc)_2·4H_2O$ (201 mg, 0.82 mmol), and 1 M NaOH (2 mL) in methanol (60 mL) was stirred at room temperature for 2 h. The resulting orange precipitate was collected by filtration, washed with cold ethanol and hexane, and dried under vacuum. Yield: 376 mg (0.75 mmol, 91%). Single crystals of **5** suitable for X-ray diffraction were obtained by crystallization from DMSO upon standing for several days, at room temperature.

DOI: 10.1021/acsomega.8b03018
ACS Omega 2019, 4, 48−57

*Synthesis of [Mn(3,5-(NO$_2$)$_2$-salpn)(H$_2$O)$_2$]·0.5H$_2$O (**6**·0.5H$_2$O).* NaOH (385 μL; 0.85 M) was added to a solution of 3,5-(NO$_2$)$_2$salpnH$_2$ (153 mg, 0.33 mmol) in methanol (100 mL) and heated under reflux. Then, a solution of 123 mg of manganese(II) perchlorate hexahydrate (0.34 mmol) in 5 mL of methanol was added and left with stirring for 1 day. The resulting ochre precipitate was collected by filtration, washed with cold methanol and hexane, and dried under vacuum. Yield: 144 mg (0.25 mmol, 76%).

*[Mn(salpn)(H$_2$O)$_2$]ClO$_4$·H$_2$O (**1**·H$_2$O).* Anal. Calcd for $C_{17}ClH_{22}MnN_2O_8\cdot H_2O$: C, 41.8; H, 4.5; Mn, 11.2; N, 5.7%. Found: C, 41.5; H, 4.2; Mn, 10.8; N, 6.1%. ESI-MS: m/z = 335.06 [**1** − 2H$_2$O − ClO$_4$]$^+$. Significant IR bands (KBr, cm^{-1}): ν_{O-H} 3382, $\nu_{C=N}$ 1605, ν_{C-O} 1296, ν_{ClO_4} 1069, ρ_{ClO_4} 617.

*[Mn(5-Cl-salpn)(H$_2$O)$_2$]ClO$_4$·H$_2$O (**2**·H$_2$O).* Anal. Calcd for $C_{17}Cl_3H_{18}MnN_2O_8\cdot H_2O$: C, 36.6; H, 3.6; N, 5.0%. Found: C, 36.3; H, 3.4; N, 5.0%. ESI-MS: m/z = 402.98 [**2** − 2H$_2$O − ClO$_4$]$^+$. Significant IR bands (KBr, cm^{-1}): ν_{O-H} 3400, $\nu_{C=N}$ 1615, ν_{C-O} 1290, ν_{ClO_4} 1092, ρ_{ClO_4} 625.

*[Mn(3,5-F$_2$-salpn)(H$_2$O)$_2$]BPh$_4$·3H$_2$O (**3**·3H$_2$O).* Anal. Calcd for $BC_{41}F_4H_{36}MnN_2O_4\cdot 3H_2O$: C, 60.3; H, 5.2; N, 3.4%. Found: C, 60.4; H, 4.9; N, 3.6%. ESI-MS: m/z = 407.02 [**3** − 2H$_2$O − BPh$_4$]$^+$. Significant IR bands (KBr, cm^{-1}): ν_{O-H} 3472 (broad), $\nu_{C=N}$ 1612, 738 (BPh$_4$), 708 (BPh$_4$), 612 (BPh$_4$).

*[Mn(3,5-Cl$_2$-salpn)(H$_2$O)$_2$]ClO$_4$·2H$_2$O (**4**·2H$_2$O).* Anal. Calcd for $C_{17}Cl_5H_{16}MnN_2O_8\cdot 2H_2O$: C, 31.6; H, 3.1; Mn, 8.5; N, 4.4%. Found: C, 31.6; H, 2.6; Mn, 8.4; N, 4.2%. ESI-MS: m/z = 473.17 [**4** − 2H$_2$O − ClO$_4$]$^+$. Significant IR bands (KBr, cm^{-1}): ν_{O-H} 3397, $\nu_{C=N}$ 1607, ν_{C-O} 1296, ν_{ClO_4} 1078, ρ_{ClO_4} 623.

*[Mn(5-(NO$_2$)-salpn)(OAc)(H$_2$O)] (**5**).* Anal. Calcd for $C_{19}H_{19}MnN_4O_9$: C, 45.4; H, 3.8; Mn, 10.9; N, 11.2%. Found: C, 45.0; H, 3.4; Mn, 11.3; N, 11.0%. ESI-MS (MeCN): m/z = 425.00 [**5** − H$_2$O − OAc]$^+$. Significant IR bands (KBr, cm^{-1}): ν_{O-H} 3403, $\nu_{C=N}$ 1639, ν_{NO_2} 1338/1557, ν_{AcO^-} 1312/1622.

*[Mn(3,5-(NO$_2$)$_2$-salpn)(H$_2$O)$_2$]·0.5H$_2$O (**6**·0.5H$_2$O).* Anal. Calcd for $C_{17}H_{16}MnN_6O_{12}\cdot 0.5H_2O$: C, 36.4; H, 3.1; N, 15.0%. Found: C, 36.1; H, 3.0; N, 14.8%. ESI-MS (DMSO/MeCN): m/z = 611.02 [**6** − H$_2$O + DMSO]$^+$. Significant IR bands (KBr, cm^{-1}): ν_{O-H} 3473 (broad), $\nu_{C=N}$ 1639, ν_{NO_2} 1525/1340.

Caution: Although we have experienced no difficulties with the perchlorate salts, they should nevertheless be regarded as hazardous and treated with care.

Physical Measurements. UV−visible spectra were recorded on a Jasco V-550 spectrophotometer, with thermostated cell compartments. EPR spectra were obtained at 115 K on an Elexsys E 500 Bruker spectrometer, operating at a microwave frequency of approximately 9.5 GHz. IR spectra were recorded on a PerkinElmer Spectrum One FT-IR spectrophotometer. Solid samples were run in attenuated total reflectance mode on a diamond crystal. Metal content was determined by atomic absorption measurements on a Metrolab 250 AA spectrophotometer. ESI-mass spectra were obtained with a Thermo Scientific LCQ Fleet. The solutions for electrospray were prepared from solutions of the complexes diluted with methanol or acetonitrile to a ≈10^{-5} M concentration. Complex **6** was initially dissolved in DMSO and then diluted with acetonitrile. ^{1}H spectra were recorded on a Bruker AC 300 NMR spectrometer at ambient probe temperature (ca. 26 °C). Chemical shifts are referenced to (CH$_3$)$_4$Si (^{1}H NMR) and downfield shifts are given a positive sign. Paramagnetic NMR spectra were acquired using super WEFT sequence, with acquisition time of 23 ms. The electrochemical experiments were performed with a computer-controlled Princeton Applied Research potentiostat, VERSASTAT II model, with the 270/250 Research Electrochemistry Software. Studies were carried out under Ar, in DMF solution using 0.1 M Bu$_4$NPF$_6$ as a supporting electrolyte and ≈10^{-3} M of the complexes. The working electrode was a glassy carbon disk, and the reference electrode was a calomel electrode isolated in a fritted bridged with a Pt wire as the auxiliary electrode. All potentials are referred to the SCE electrode. Under these conditions, $E_{(ferrocene/ferrocenium)}$ = 474 mV, in DMF.

Indirect SOD Assay. The SOD-like activity of the complexes was evaluated by measuring the inhibition of the reduction of NBT by $O_2^{\bullet-}$ spectrophotometrically.[65] The reaction mixtures contained riboflavin (3.25 × 10^{-6} M), methionine (9.65 × 10^{-3} M), NBT (3.82 × 10^{-5} M), and complex (different concentrations), in phosphate buffer (pH 7.8). Riboflavin was added last and the mixtures were illuminated during 30 min with an 18 W fluorescent lamp placed at 15 cm, at 25 °C. The reduction of NBT was measured at 560 nm, and the IC$_{50}$ values were determined graphically. Control reactions confirmed that the compounds did not react directly with NBT or riboflavin. Inhibition percentage was calculated according to: $\{(\Delta Abs/t)_{without\ complex} - (\Delta Abs/t)_{with\ complex}\} \times 100/(\Delta Abs/t)_{without\ complex}$. At 50% inhibition of NBT reduction, k_{McF} [complex] = k_{NBT} [NBT], where k_{NBT} (pH = 7.8) = 5.94 × 10^4 M^{-1} s^{-1}, and k_{McF} can be calculated.[50,66]

EPR Measurements in DMSO. A mixture of **1** (1.25 mM) and KO$_2$ (1.2 mM) in DMSO was left to react and aliquots were extracted at different times and frozen in N$_2$(l) for EPR measurements. For **5** + KO$_2$, the concentrations were 0.75 and 1.1 mM, respectively.

A mixture of 0.16 mL of a DMSO solution of **6** (1.6 mM) and 0.1 mL of saturated solution of KO$_2$ (with excess solid KO$_2$) was left to react and aliquots were extracted at different times and frozen in N$_2$(l) for EPR measurements.

Stock KO$_2$ solution in anhydrous DMSO was prepared by mixing 9.3 mg of KO$_2$ in DMSO (5 mL) and sonicated for 15 min, followed by centrifugation at 6000 rpm during 25 min. The concentration of KO$_2$ in the supernatant was estimated by using its extinction coefficient 2686 M^{-1} cm^{-1} in deoxygenated DMSO solution[67] and confirmed by the horseradish peroxidase assay.

Crystal Data Collection and Refinement. Single-crystal data were collected on an Oxford Diffraction Gemini E CCD diffractometer equipped with a sealed tube with Mo Kα radiation (λ = 0.71073 Å). Crystal structure data were corrected for absorption with CrysAlisPro, Agilent Technologies, version 1.171.34.49, applying an empirical absorption correction using spherical harmonics, implemented in SCALE3 ABSPACK scaling algorithm. The structure was solved by Patterson methods with SHELXS-97[68] and refined by full-matrix least-squares on F2 with SHELXL-97.[69] All non-hydrogen atoms were refined anisotropically and hydrogen atoms were added geometrically and refined as riding atoms with a uniform value of U$_{iso}$. Crystal data collection and refinement parameters for compound **5** are summarized in Table S2.

DOI: 10.1021/acsomega.8b03018
ACS Omega 2019, 4, 48−57

■ ASSOCIATED CONTENT

Supporting Information

The Supporting Information is available free of charge on the ACS Publications website at DOI: 10.1021/acsomega.8b03018.

Synthesis of complexes **1**−**4**, IR spectra of complexes **1**−**6**, ESI-mass spectra of complexes **1**−**6**, ^{1}H NMR spectra of complexes **1**−**4** in D_4-methanol, ESI-mass spectrum of $[Mn_2(salpn)_2(O)_2]$, electrochemical parameters for complexes **1**−**6** in V versus SCE, and crystal data for $[Mn(5\text{-}(NO_2)\text{-salpn})(OAc)(H_2O)]$ (**5**). Full crystallographic data for **5** are available at the Cambridge Crystallographic Data Center (Deposit number: CCDC-1877167) (PDF)

■ AUTHOR INFORMATION

Corresponding Author

*E-mail: signorella@iquir-conicet.gov.ar (S.R.S.).

ORCID

Elodie Anxolabéhère-Mallart: 0000-0002-8708-802X

Sandra R. Signorella: 0000-0002-1547-6891

Notes

The authors declare no competing financial interest.

■ ACKNOWLEDGMENTS

This work was supported by the National University of Rosario and the Consejo Nacional de Investigaciones Científicas y Técnicas (CONICET, PIP 0337), the Centre National de la Recherche Scientifique (CNRS, PICS 07121), CONICET/CNRS bilateral agreement (Res. 991/13), and the Agency for Science, Technology and Innovation of Santa Fe (ASACTeI, IO 2010-164-16). We thank Regina Colagioia and Facundo Farabolini for SOD determinations, Fabrice Collin and Laurent Sabater for ESI-MS, and Lionel Rechignat for EPR measurements.

■ REFERENCES

(1) Abreu, I. A.; Cabelli, D. E. Superoxide dismutases-a review of the metal-associated mechanistic variations. *Biochim. Biophys. Acta* **2010**, *1804*, 263−274.

(2) Sheng, Y.; Abreu, I. A.; Cabelli, D. E.; Maroney, M. J.; Miller, A.-F.; Teixeira, M.; Valentine, J. S. Superoxide dismutases and superoxide reductases. *Chem. Rev.* **2014**, *114*, 3854−3918.

(3) Rhee, S. G.; Chang, T.-S.; Jeong, W.; Kang, D. Methods for detection and measurement of hydrogen peroxide inside and outside of cells. *Mol. Cells* **2010**, *29*, 539−549.

(4) Cheignon, C.; Tomas, M.; Bonnefont-Rousselot, D.; Faller, P.; Hureau, C.; Collin, F. Oxidative stress and the amyloid beta peptide in Alzheimer's disease. *Redox Biol.* **2018**, *14*, 450−464.

(5) Day, B. J. Catalase and glutathione peroxidase mimics. *Biochem. Pharmacol.* **2009**, *77*, 285−296.

(6) Batinic-Haberle, I.; Tovmasyan, A.; Roberts, E. R. H.; Vujaskovic, Z.; Leong, K. W.; Spasojevic, I. SOD therapeutics: latest insights into their structure-activity relationships and impact on the cellular redox-based signaling pathways. *Antioxid. Redox Signaling* **2014**, *20*, 2372−2415.

(7) Policar, C. Mimicking SOD, Why and How: Bio-Inspired Manganese Complexes as SOD Mimic. In *Redox Active Therapeutics*; Reboucas, J. S., Batinic-Haberle, I., Spasojevic, I., Warner, D. S., St. Clair, D., Eds.; Springer: Berlin, 2016; pp 125−164.

(8) Mjos, K. D.; Orvig, C. Metallodrugs in medicinal inorganic chemistry. *Chem. Rev.* **2014**, *114*, 4540−4563.

(9) Cuzzocrea, S.; Riley, D.P.; Caputi, A.P.; Salvemini, D. Antioxidant therapy: a new pharmacological approach in shock, inflammation, and ischemia/reperfusion injury. *Pharmacol Rev.* **2001**, *53*, 135−159.

(10) Anderson, C. M.; Allen, B. G.; Sun, W.; Lee, C. M.; Agarwala, S.; Venigalla, M.; Greenberg, L.; Adkins, D.; Chen, Y.; Zhen, W.; Mould, D.; Holmlund, J.; Brill, J.; Sonis, S.; Buatti, J. Phase 1b/2a trial of superoxide (SO) dismutase (SOD) mimetic GC4419 to reduce chemoradiation therapy−induced oral mucositis (OM) in patients with oral cavity or oropharyngeal carcinoma (OCC). *Int. J. Radiat. Oncol., Biol., Phys.* **2016**, *94*, 869−870.

(11) Kinnula, V. L.; Crapo, J. D. Superoxide dismutases in the lung and human lung diseases. *Am. J. Respir. Crit. Care Med.* **2003**, *167*, 1600−1619.

(12) Rong, Y.; Doctrow, S. R.; Tocco, G.; Baudry, M. EUK-134, a synthetic superoxide dismutase and catalase mimetic, prevents oxidative stress and attenuates kainate-induced neuropathology. *Proc. Natl. Acad. Sci. U.S.A.* **1999**, *96*, 9897−9902.

(13) Brazier, M. W.; Doctrow, S. R.; Masters, C. L.; Collins, S. J. A manganese-superoxide dismutase/catalase mimetic extends survival in a mouse model of human prion disease. *Free Radical Biol. Med.* **2008**, *45*, 184−192.

(14) Doctrow, S.; Liesa, M.; Melov, S.; Shirihai, O.; Tofilon, P. Salen Mn complexes are superoxide dismutase/catalase mimetics that protect the mitochondria. *Curr. Inorg. Chem.* **2012**, *2*, 325−334.

(15) Signorella, S.; Palopoli, C.; Ledesma, G. Rationally designed mimics of antioxidant manganoenzymes: Role of structural features in the quest for catalysts with catalase and superoxide dismutase activity. *Coord. Chem. Rev.* **2018**, *365*, 75−102.

(16) Bosch, S.; Comba, P.; Gahan, L. R.; Schenk, G. Dinuclear Zinc(II) complexes with hydrogen bond donors as structural and functional phosphatase models. *Inorg. Chem.* **2014**, *53*, 9036−9051.

(17) Camargo, T. P.; Neves, A.; Peralta, R. A.; Chaves, C.; Maia, E. C. P.; Lizarazo-Jaimes, E. H.; Gomes, D. A.; Bortolotto, T.; Norberto, D. R.; Terenzi, H.; Tierney, D. L.; Schenk, G. Second-sphere effects in dinuclear $Fe^{III}Zn^{II}$ hydrolase biomimetics: Tuning binding and reactivity properties. *Inorg. Chem.* **2017**, *57*, 187−203.

(18) Erxleben, A. Transition metal salen complexes in bioinorganic and medicinal chemistry. *Inorg. Chim. Acta* **2018**, *472*, 40−57.

(19) Larson, E. J.; Pecoraro, V. L. The peroxide-dependent μ2-O bond formation of manganese complex [Mn(IV)SALPN(O)]2. *J. Am. Chem. Soc.* **1991**, *113*, 3810−3818.

(20) Bermejo, M. R.; Fondo, M.; Garcia-Deibe, A.; Rey, M.; Sanmartin, J.; Sousa, A.; Watkinson, M.; McAuliffe, C. A.; Pritchard, R. G. The diversity observed in manganese(III) complexes of tetradentate Schiff base ligands: An assessment of structural trends. *Polyhedron* **1996**, *15*, 4185−4194.

(21) Vázquez-Fernández, M. Á.; Bermejo, M. R.; Fernández-García, M. I.; González-Riopedre, G.; Rodríguez-Doutón, M. J.; Maneiro, M. Influence of the geometry around the manganese ion on the peroxidase and catalase activities of Mn(III)−Schiff base complexes. *J. Inorg. Biochem.* **2011**, *105*, 1538−1547.

(22) Maneiro, M.; Bermejo, M. R.; Fondo, M.; González, A. M.; Sanmartín, J.; García-Monteagudo, J. C.; Pritchard, R. G.; Tyryshkin, A. M. Structural and photolytic studies on new mononuclear and binuclear manganese complexes containing Schiff base ligands. The crystal structure of [Mn(μ-3,5-Brsalpn)(μ-O)]2·2DMF. *Polyhedron* **2001**, *20*, 711−719.

(23) Palopoli, C.; Gómez, G.; Foi, A.; Doctorovich, F.; Mallet-Ladeira, S.; Hureau, C.; Signorella, S. Dimerization, redox properties and antioxidant activity of two manganese(III) complexes of difluoro- and dichloro-substituted Schiff-base ligands. *J. Inorg. Biochem.* **2017**, *167*, 49−59.

(24) Bonadies, J. A.; Maroney, M. J.; Pecoraro, V. L. Structurally diverse manganese(III) Schiff base complexes: solution speciation via paramagnetic proton NMR spectroscopy and electrochemistry. *Inorg. Chem.* **1989**, *28*, 2044−2051.

(25) Caudle, M. T.; Riggs-Gelasco, P.; Gelasco, A. K.; Penner-Hahn, J. E.; Pecoraro, V. L. Mechanism for the homolytic cleavage of alkyl hydroperoxides by the manganese(III) dimer MnIII2(2-OHsalpn)2. *Inorg. Chem.* **1996**, *35*, 3577−3584.

DOI: 10.1021/acsomega.8b03018
ACS Omega 2019, 4, 48−57

(26) Hoogenraad, M.; Ramkisoensing, K.; Driessen, W. L.; Kooijman, H.; Spek, A. L.; Bouwman, E.; Haasnoot, J. G.; Reedijk, J. Catalytic and electrochemical properties of new manganese(III) compounds of 2-(2′-hydroxyphenyl)-oxazoline (Hphox or HClphox). Molecular structures of [Mn(Clphox)2(MeOH)2](ClO4) and [Mn-(phox)2(MeOH)2][Mn(phox)2(ClO4)2] (H2O)2. *Inorg. Chim. Acta* **2001**, *320*, 117−126.
(27) Shova, S.; Vlad, A.; Cazacu, M.; Krzystek, J.; Bucinsky, L.; Breza, M.; Darvasiová, D.; Rapta, P.; Cano, J.; Telser, J.; Arion, V. B. A five-coordinate manganese(III) complex of a salen type ligand with a positive axial anisotropy parameter D. *Dalton Trans.* **2017**, *46*, 11817−11829.
(28) Tadyszak, K.; Rudowicz, C.; Ohta, H.; Sakurai, T. Electron magnetic resonance data on high-spin Mn(III; S = 2) ions in porphyrinic and salen complexes modeled by microscopic spin Hamiltonian approach. *J. Inorg. Biochem.* **2017**, *175*, 36−46.
(29) Gahan, L. R.; Grillo, V. A.; Hambley, T. W.; Hanson, G. R.; Hawkins, C. J.; Proudfoot, E. M.; Moubaraki, B.; Murray, K. S.; Wang, D. Synthetic, X-ray structure, electron paramagnetic resonance, and magnetic studies of the manganese(II) complex of 1-thia-4,7-diazacyclononane ([9]aneN2S). *Inorg. Chem.* **1996**, *35*, 1039−1044.
(30) Groni, S.; Hureau, C.; Guillot, R.; Blondin, G.; Blain, G.; Anxolabéhère-Mallart, E. Characterizations of chloro and aqua Mn(II) mononuclear complexes with amino-pyridine ligands. Comparison of their electrochemical properties with those of Fe(II) counterparts. *Inorg. Chem.* **2008**, *47*, 11783−11797.
(31) Hureau, C.; Blondin, G.; Charlot, M.-F.; Philouze, C.; Nierlich, M.; Césario, M.; Anxolabéhère-Mallart, E. Synthesis, structure, and characterization of new mononuclear Mn(II) complexes. Electrochemical conversion into new oxo-bridged Mn2(III,IV) complexes. Role of chloride ions. *Inorg. Chem.* **2005**, *44*, 3669−3683.
(32) Hureau, C.; Groni, S.; Guillot, R.; Blondin, G.; Duboc, C.; Anxolabéhère-Mallart, E. Syntheses, X-ray structures, solid state high-field electron paramagnetic resonance, and density-functional theory investigations on chloro and aqua MnII mononuclear complexes with amino-pyridine pentadentate ligands. *Inorg. Chem.* **2008**, *47*, 9238−9247.
(33) Takahata, Y.; Chong, D. P. Estimation of Hammett sigma constants of substituted benzenes through accurate density-functional calculation of core-electron binding energy shifts. *Int. J. Quantum Chem.* **2005**, *103*, 509−515.
(34) Hureau, C.; Sabater, L.; Gonnet, F.; Blain, G.; Sainton, J.; Anxolabéhère-Mallart, E. Chemical access to the mononuclear Mn(III) [(mL)Mn(OMe)]+ complex (mLH = N,N′-bis-(2-pyridyl-methyl)-N-(2-hydroxybenzyl)-N′-methyl-ethane-1,2-diamine) and electrochemical oxidation to the Mn(IV) [(mL)Mn(OMe)]2+ species. *Inorg. Chim. Acta* **2006**, *359*, 339−345.
(35) Dubois, L.; Xiang, D.-F.; Tan, X.-S.; Pécaut, J.; Jones, P.; Baudron, S.; Le Pape, L.; Latour, J.-M.; Baffert, C.; Chardon-Noblat, S.; Collomb, M.-N.; Deronzier, A. Binuclear manganese compounds of potential biological significance. Syntheses and structural, magnetic, and electrochemical properties of dimanganese(II) and -(II,III) complexes of a bridging unsymmetrical phenolate ligand. *Inorg. Chem.* **2003**, *42*, 750−760.
(36) Bermejo, M. R.; González, A. M.; Fondo, M.; García-Deibe, A.; Maneiro, M.; Sanmartín, J.; Hoyos, O. L.; Watkinson, M. A direct route to obtain manganese(III) complexes with a new class of asymmetrical Schiff base ligands. *New J. Chem.* **2000**, *24*, 235−241.
(37) Bermejo, M. R.; González-Noya, A. M.; Abad, V.; Fernández, M. I.; Maneiro, M.; Pedrido, R.; Vásquez, M. Formation of novel 1-D chains by μ-amido bridging of dinuclear manganese(III)-Schiff base complexes. *Eur. J. Inorg. Chem.* **2004**, 3696−3705.
(38) Li, X.; Pecoraro, V. L. Stepwise, metal-assisted decarboxylation promoted by manganese: reactivity relationship between manganese and vanadium. *Inorg. Chem.* **1989**, *28*, 3403−3410.
(39) González-Riopedre, G.; Fernández-García, M.; Gómez-Fórneas, E.; Maneiro, M. Biomimetic catalysts for oxidation of veratryl alcohol, a lignin model compound. *Catalysts* **2013**, *3*, 232−246.
(40) Bermejo, M. R.; Castiñeiras, A.; Garcia-Monteagudo, J. C.; Rey, M.; Sousa, A.; Watkinson, M.; McAuliffe, C. A.; Pritchard, R. G.; Beddoes, R. L. Electronic and steric effects in manganese Schiff-base complexes as models for the water oxidation complex in photosystem II. The isolation of manganese-(II) and -(III) complexes of 3- and 3,5-substituted N,N′-bis(salicylidene)ethane-1,2-diamine (H_2salen) ligands. *J. Chem. Soc., Dalton Trans.* **1996**, 2935−2944.
(41) Doctrow, S. R.; Huffman, K.; Marcus, C. B.; Tocco, G.; Malfroy, E.; Adinolfi, C. A.; Kruk, H.; Baker, K.; Lazarowych, N.; Mascarenhas, J.; Malfroy, B. Salen−manganese complexes as catalytic scavengers of hydrogen peroxide and cytoprotective agents: Structure−activity relationship studies. *J. Med. Chem.* **2002**, *45*, 4549−4558.
(42) Watanabe, Y.; Namba, A.; Umezawa, N.; Kawahata, M.; Yamaguchi, K.; Higuchi, T. Enhanced catalase-like activity of manganese salen complexes in water: effect of a three-dimensionally fixed auxiliary. *Chem. Commun.* **2006**, 4958−4960.
(43) Moreno, D.; Daier, V.; Palopoli, C.; Tuchagues, J.-P.; Signorella, S. Synthesis, characterization and antioxidant activity of water soluble MnIII complexes of sulphonato-substituted Schiff base ligands. *J. Inorg. Biochem.* **2010**, *104*, 496−502.
(44) Bian, H.-D.; Wang, J.; Wei, Y.; Tang, J.; Huang, F.-P.; Yao, D.; Yu, Q.; Liang, H. Superoxide dismutase activity studies of Mn(III)/Cu(II)/Ni(II) complexes with Schiff base ligands. *Polyhedron* **2015**, *90*, 147−153.
(45) Zhang, X.-M.; Tang, J.; Wang, L.-N.; Yao, D.; Yu, Q.; Huang, F.-P.; Bian, H.-D. Superoxide dismutase activity studies of Mn(III)/Co(III)/Fe(III) complexes with Schiff base ligands. *Polyhedron* **2017**, *133*, 433−440.
(46) Daier, V.; Moreno, D.; Duhayon, C.; Tuchagues, J.-P.; Signorella, S. Synthesis, characterization and combined superoxide dismutase and catalase activities of manganese complexes of 1,4-bis(salicylidenamino)butan-2-ol. *Eur. J. Inorg. Chem.* **2010**, *2010*, 965−974.
(47) Signorella, S.; Daier, V.; Ledesma, G.; Palopoli, C.; Back, D. F.; Lang, E. S.; Kopp, C. R.; Ebani, P.; Pereira, M. B.; Giacomelli, C.; Piquini, P. C. Synthesis, structure and SOD activity of Mn complexes with symmetric Schiff base ligands derived from pyridoxal. *Polyhedron* **2015**, *102*, 176−184.
(48) Costa, R. O.; Ferreira, S. S.; Pereira, C. A.; Harmer, J. R.; Noble, C. J.; Schenk, G.; Franco, R. W. A.; Resende, J. A. L. C.; Comba, P.; Roberts, A. E.; Fernandes, C.; Horn, A., Jr A new mixed-valence Mn(II)Mn(III) compound with catalase and superoxide dismutase activities. *Front. Chem.* **2018**, *6*, 491.
(49) Durot, S.; Policar, C.; Cisnetti, F.; Lambert, F.; Renault, J.-P.; Pelosi, G.; Blain, G.; Korri-Youssoufi, H.; Mahy, J.-P. Series of Mn complexes based on *N*-centered ligands and superoxide reactivity in an anhydrous medium and SOD-like activity in an aqueous medium correlated to Mn^{II}/Mn^{III} redox potentials. *Eur. J. Inorg. Chem.* **2005**, *2005*, 3513−3523.
(50) Batinic-Haberle, I.; Spasojevic, I.; Stevens, R. D.; Hambright, P.; Neta, P.; Okado-Matsumoto, A.; Fridovich, I. New class of potent catalysts of $O_2^{\cdot-}$ dismutation. Mn(III) ortho-methoxyethylpyridyl- and di-ortho-methoxyethylimidazolylporphyrins. *Dalton Trans.* **2004**, 1696−1702.
(51) Lieb, D.; Friedel, F. C.; Yawer, M.; Zahl, A.; Khusniyarov, M. M.; Heinemann, F. W.; Ivanović-Burmazović, I. Dinuclear seven-coordinate Mn(II) complexes: effect of manganese(II)-hydroxo species on water exchange and superoxide dismutase activity. *Inorg. Chem.* **2012**, *52*, 222−236.
(52) Campbell, K. A.; Lashley, M. R.; Wyatt, J. K.; Nantz, M. H.; Britt, R. D. Dual-mode EPR study of Mn(III) salen and the Mn(III) salen-catalyzed epoxidation of *cis*-β-methylstyrene. *J. Am. Chem. Soc.* **2001**, *123*, 5710−5719.
(53) Schäfer, K.-O.; Bittl, R.; Lendzian, F.; Barynin, V.; Weyhermüller, T.; Wieghardt, K.; Lubitz, W. Multifrequency EPR investigation of dimanganese catalase and related Mn(III)Mn(IV) complexes. *J. Phys. Chem. B* **2003**, *107*, 1242−1250.

DOI: 10.1021/acsomega.8b03018
ACS Omega 2019, 4, 48−57

(54) Hureau, C.; Blondin, G.; Cesario, M.; Un, S. Direct measurement of the hyperfine and *g*-tensors of a Mn(III)−Mn(IV) complex in polycrystalline and frozen solution samples by high-field EPR. *J. Am. Chem. Soc.* **2003**, *125*, 11637−11645.
(55) Hureau, C.; Blanchard, S.; Nierlich, M.; Blain, G.; Rivière, E.; Girerd, J.-J.; Anxolabéhère-Mallart, E.; Blondin, G. Controlled redox conversion of new X-ray-characterized mono- and dinuclear heptacoordinated Mn(II) complexes into di-μ-oxo-dimanganese core complexes. *Inorg. Chem.* **2004**, *43*, 4415−4426.
(56) Larson, E. J.; Riggs, P. J.; Penner-Hahn, J. E.; Pecoraro, V. L. Protonation of $[\{Mn^{IV}(saltn)(\mu\text{-}O)\}_2]$ results in significant modification of structure and catalase-like reactivity. *J. Chem. Soc., Chem. Commun.* **1992**, 102−103.
(57) Bagchi, R. N.; Bond, A. M.; Scholz, F.; Stoesser, R. Characterization of the ESR spectrum of the superoxide anion in the liquid phase. *J. Am. Chem. Soc.* **1989**, *111*, 8270−8271.
(58) Ivanović-Burmazović, I.; van Eldik, R. Metal complex-assisted activation of small molecules. From NO to superoxide and peroxides. *Dalton Trans.* **2008**, 5259−5275.
(59) Liu, G.-F.; Filipović, M.; Heinemann, F. W.; Ivanović-Burmazović, I. Seven-coordinate iron and manganese complexes with acyclic and rigid pentadentate chelates and their superoxide dismutase activity. *Inorg. Chem.* **2007**, *46*, 8825−8835.
(60) Liu, G.-F.; Dürr, K.; Puchta, R.; Heinemann, F. W.; van Eldik, R.; Ivanović-Burmazović, I. Chelate electronic properties control the redox behaviour and superoxide reactivity of seven-coordinate manganese(II) complexes. *Dalton Trans.* **2009**, 6292−6295.
(61) Hong, S.; Sutherlin, K. D.; Park, J.; Kwon, E.; Siegler, M. A.; Solomon, E. I.; Nam, W. Crystallographic and spectroscopic characterization and reactivities of a mononuclear non-haem iron-(III)-superoxo complex. *Nat. Commun.* **2014**, *5*, 5440.
(62) Maroz, A.; Kelso, G. F.; Smith, R. A. J.; Ware, D. C.; Anderson, R. F. Pulse radiolysis investigation on the mechanism of the catalytic action of Mn(II)−pentaazamacrocycle compounds as superoxide dismutase mimetics. *J. Phys. Chem. A* **2008**, *112*, 4929−4935.
(63) Leto, D. F.; Chattopadhyay, S.; Day, V. W.; Jackson, T. A. Reaction landscape of a pentadentate N5-ligated Mn^{II} complex with $O_2^{\cdot-}$ and H_2O_2 includes conversion of a peroxomanganese(III) adduct to a bis(μ-oxo)dimanganese(III,IV) species. *Dalton Trans.* **2013**, *42*, 13014−13025.
(64) Gohdes, J. W.; Armstrong, W. H. Synthesis, structure, and properties of [Mn(salpn)(EtOH)2](ClO4) and its aerobic oxidation product [Mn(salpn)O]2. *Inorg. Chem.* **1992**, *31*, 368−373.
(65) Beauchamp, C.; Fridovich, I. Superoxide dismutase: improved assays and an assay applicable to acrylamide gels. *Anal. Biochem.* **1971**, *44*, 276−287.
(66) Liao, Z.-R.; Zheng, X.-F.; Luo, B.-S.; Shen, L.-R.; Li, D.-F.; Liu, H.-L.; Zhao, W. Synthesis, characterization and SOD-like activities of manganese-containing complexes with N,N,N′,N′-tetrakis(2′-benzimidazolylmethyl)-1,2-ethanediamine (EDTB). *Polyhedron* **2001**, *20*, 2813−2821.
(67) Hyland, K.; Auclair, C. The formation of superoxide radical anions by a reaction between O2, OH− and dimethyl sulfoxide. *Biochem. Biophys. Res. Commun.* **1981**, *102*, 531−537.
(68) Sheldrick, G. M. *Program for the Refinement of crystal structures from diffraction data*; University of Göttingen: Göttingen, Germany, 1997.
(69) Sheldrick, G. M. Crystal structure refinement with SHELXL. *Acta Crystallogr., Sect. C: Struct. Chem.* **2015**, *71*, 3−8.

DOI: 10.1021/acsomega.8b03018
ACS Omega 2019, 4, 48−57